Groundwater

Influence of Alluvial Morphology on Upscaled Hydraulic Conductivity

by Sanjeev Kumar Jha[1,2], Gregoire Mariethoz[3], George Mathews[4], John Vial[4], and Bryce F.J. Kelly[5]

Abstract

The hydraulic conductivity of aquifers is a key parameter controlling the interactions between resource exploitation activities, such as unconventional gas production and natural groundwater systems. Furthermore, this parameter is often poorly constrained by typical data used for regional groundwater modeling and calibration studies performed as part of impact assessments. In this study, a systematic investigation is performed to understand the correspondence between the lithological descriptions of channel-type formation and the bulk effective hydraulic conductivities at a larger scale (Kx_{eff}, Ky_{eff}, and Kz_{eff} in the direction of channel cross section, along the channel and in the vertical directions, respectively). This will inform decisions on what additional data gathering and modeling of the geological system can be performed to allow the critical bulk properties to be more accurately predicted. The systems studied are conceptualized as stacked meandering channels formed in an alluvial plain, and are represented as two facies. Such systems are often studied using very detailed numerical models. The main factors that may influence Kx_{eff}, Ky_{eff}, and Kz_{eff} are the proportion of the facies representing connected channels, the aspect ratio of the channels, and the difference in hydraulic conductivity between facies. Our results show that in most cases, Kz_{eff} is only weakly dependent on the orientations of channelized structures, with the main effects coming from channel aspect ratio and facies proportion.

Introduction

The hydraulic conductivity of aquifers (K) is a critical hydraulic parameter in assessing the impact of anthropogenic activities such as underground mine development and unconventional gas production, which may result in the depressurization of adjacent aquifers. The magnitude of K in the vertical direction (Kz) plays a critical role in interaction with surface processes (e.g., recharge rates and susceptivity to contamination from above). Kz also controls how the deep dewatering or depressurization affects the flow in the overlying groundwater systems (Chen 1997; Hart et al. 2006). For these deep geological units, there is often insufficient direct head and flow information to allow the critical bulk hydraulic parameters to be accurately estimated using a regional scale calibration process. This is further complicated by the presence of complex and heterogeneous geological formations (e.g., in the Murray-Darling Basin in Australia, Moran and Vink [2010]). To perform detailed hydrogeological analysis of flow through heterogeneous geological formations, an excessively large number of grid cells would be required (Szymkiewicz 2013). To overcome this, the standard approach consists of estimating K for a larger block of aquifer referred to as bulk effective hydraulic conductivity (Kx_{eff}, Ky_{eff}, and Kz_{eff} in the direction of channel cross section, along the channel and in the vertical directions, respectively). Upscaling is used to translate properties from a detailed description of geological heterogeneity to a larger scale groundwater flow model. The number of grid cells is thus reduced without losing the important hydrofacies structural features (Fleckenstein and Fogg 2008). Upscaling therefore helps to overcome limitations related to the computational cost and memory storage. Extensive reviews about upscaling methods are presented by Wen and Gómez-Hernández (1996) and Sanchez-Vila et al. (2006).

This study focuses on investigating alluvial formations, which are often represented as permeable paleochannels (e.g., sandstone or conglomerate) in a less permeable matrix (e.g., claystone or siltstone), and where groundwater flow paths are influenced by the connection among hydrofacies formed by the high permeability material (Renard et al. 2011). Without considering a particular site, we perform geological modeling experiments

[1]Currently at the Bureau of Meteorology, 14 Childers Street, Canberra, ACT 6201, Australia.
[2]Corresponding author: School of Civil and Environmental Engineering, UNSW, Sydney, Australia; jha.sanj@gmail.com
[3]Institute of Earth Surface Dynamics, University of Lausanne, Lausanne, Switzerland.
[4]National ICT Australia, Sydney, Australia.
[5]Connected Waters Initiative Research Centre, National Centre for Groundwater Research and Training, UNSW Australia, Sydney, Australia.

Received February 2015, accepted August 2015.

doi: 10.1111/gwat.12378

to inform the important morphological characteristics of the paleochannels which govern the bulk effective hydraulic conductivities. The detailed modeling of these structures is challenging and has received a lot of attention recently (Deutsch and Tran 2002; Arpat and Caers 2007; Hill and Griffiths 2009).

There is a large body of literature that uses percolation theory to show that the rate of flow depends not only on connected pathways between high permeability materials but also on the geometry of the channels (Andrade et al. 2000; Hunt 2001; Hunt and Idriss 2009; Ronayne and Gorelick 2006). If highly permeable materials are randomly placed in a geological unit, the percolation is known to occur when the proportion of high permeability material is 0.3116 or higher (Stauffer and Aharony 1992). However, several studies (e.g., Harter 2005; Guin and Ritzi 2008) analyze the relationship between the geological structure and the percolation threshold to demonstrate that percolation depends on the spatial characteristics of geological facies. The percolation threshold may occur at a much lower sand proportion when for example elongated connected geobodies are considered (Dell'Arciprete et al. 2014). In a naturally deposited channel belt, the preferential flow paths may be due to connected gravels placed in different strata (Guin et al. 2010; Ramanathan et al. 2010). Therefore, the nature of the connected clusters may change with the levels of strata considered in the study. Ronayne et al. (2008) studied the flow and transport behavior of an alluvial fan system containing discrete channels deposits to identify the nature of channelized structures which form conduits and changes the system's response to pumping. These studies highlight the importance of realistically depicting sedimentary architectures when modeling flow in heterogeneous aquifers.

The flow in channelized geological units is driven by the contrast between the permeable channels and the less permeability surrounding material, the number of channels (proportion of sand or channel facies), and the shape of the individual channels. The rationale of our approach is to investigate in a systematic way how Kx_{eff}, Ky_{eff}, and Kz_{eff} are affected by different channel geometries and hydraulic properties, and determine which parameters are critical. We are not replicating geology of any particular site or matching any natural deposits. Instead, our goal is to investigate how the geometry of the channelized structures and associated connectivity influences Kx_{eff}, Ky_{eff}, and Kz_{eff}. This will enable better data gathering and modeling decisions to be made to predict the bulk effective hydraulic conductivities for a specific site when it is unconstrained by a regional groundwater calibration study.

This article is organized as follows: the methodologies to obtain three dimensional (3D) facies models are briefly described in section "Generating 3D Facies Model." The set-up of the groundwater model to estimate bulk effective hydraulic conductivity is provided in section "Determining the Bulk Effective Hydraulic Conductivity." Results are discussed in the "Results and Discussion" section, and conclusions are presented in the "Conclusions" section.

Generating 3D Facies Models

Among many methods of generating 3D facies models, we use in this study a multiple-point-based geostatistical simulation (MPS) approach (Strebelle 2002) and an object-based simulations (OBS) method (Haldorsen and Chang 1986; Falivene et al. 2007). MPS is based on the use of a training image to infer high-order statistics. It can create continuous or discontinuous and highly heterogeneous distributions of high and low permeability materials. In this study, the training image is used in such a way that the channels obtained from MPS are not as connected as those generated using the OBS approach. Both approaches allow parameterizing the channel geometry such that it is possible to investigate the effect of different types of channelized structures on the aggregated vertical flow behavior. For comparison, we also generate facies models with a Bernoulli noise model, which populates the cells of the geological model with a facies type independently of all other cells.

The methodology to obtain the 3D facies models using MPS is described in detail in Jha et al. (2014) and is briefly presented in Figures 1 and 2. The first step involves specifying a set of 2D channel cross sections. In this study, we investigate sand proportions ranging from 10% to 80%. Another important morphological characteristic of the channels is their aspect ratio, defined as the ratio between the width and the depth of the channel. There are three sets of 2D sketches presented in Figure 1a to 1c with average channel aspect ratio of 5, 20, and 50, respectively. These values of channel aspect ratio are chosen based on the extensive observations of real-world channels by Gibling (2006). By changing the aspect ratio, we obtain a set of scenarios ranging from narrow deep channels (Figure 1a), to broad shallow channels (Figure 1c), with more equant channels in between (Figure 1b).

Next, 3D volumes are generated by extruding the 2D sketches in the y direction. The resulting 3D volumes from the 2D sketches of Figure 1a are shown in Figure 1d. These 3D volumes are then used as training images to perform MPS simulation. In addition, the MPS methodology allows for the application of rotation parameters (α_{MPS} and ε_{MPS}) to generate different channelized structures (Mariethoz and Kelly 2011). The median rotation (α_{MPS}) affects the overall orientation of the channels and the rotation tolerance (ε_{MPS}) affects the local meandering patterns allowing channels to rotate between $\alpha_{\text{MPS}} - \varepsilon_{\text{MPS}}$ and $\alpha_{\text{MPS}} + \varepsilon_{\text{MPS}}$. Figure 2a shows four MPS simulations with a 30% sand proportion, a median rotation of $\alpha_{\text{MPS}} = 0^{\circ}$, and different rotation tolerances of $\varepsilon_{\text{MPS}} = 0^{\circ}$, 30°, 60°, and 90° to obtain different degrees of randomness in the organization of the channels.

In addition to MPS, we also obtain object-based models by using TiGenerator (Maharaja 2008). Objects are parameterized as sinusoidal shapes with fixed dimensions

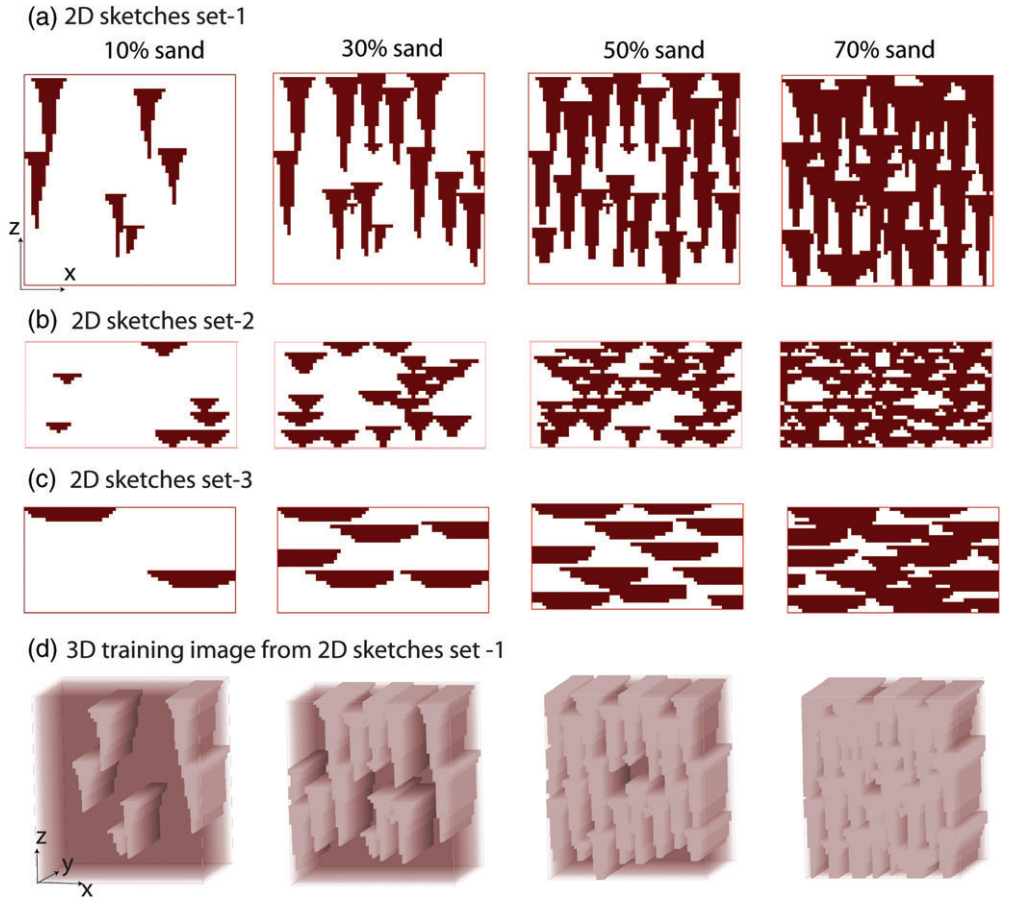

Figure 1. Sample of simulations based on multiple-point statistics (MPS) simulation. (a) to (c) represent three sets of 2D sketches with channels in an aquifer with aspect ratio 5, 20, and 50 respectively; (d) sample of extruded 2D sketches into 3D training images to use in MPS.

(length, width, thickness, amplitude, and wavelength) and varying orientations. A uniform distribution is chosen for the channel orientation with minimum and maximum values of $-\varepsilon_{OBS}$ to $+\varepsilon_{OBS}$. It is worth pointing out that a different orientation is drawn for each channel. There is a difference in the way rotation of the channels are parameterized in MPS and OBS models; their effects on the generated models are different. Four sample OBS model simulations are shown in Figure 2b. The 2D cross section of three sets of OBS models is presented in the Figure S1, Supporting Information. The overall meaning of ε is that it controls the anisotropy of the generated models. If the range of ε is large, then the channels are positioned in random directions for both types of models, resulting in horizontally isotropic models. Conversely, using a small range of ε results in channels being parallel in both MPS and OBS models, hence a strong level of anisotropy in the resulting models.

Using both MPS and OBS methods, we generate models that systematically investigate a large number of combinations of parameter values. As a result, we obtain an ensemble of models representative of a spectrum of channelized geological structures. The parameters used in both approaches to generate the 3D facies models are listed in Table 1. For each parameter set, 30 realizations are produced, resulting in a total of 2880 ($30 \times 4 \times 8 \times 3$) 3D binary models of channelized structures for MPS and another 2880 models using the object-based method, making a total of 5760 models.

In addition, we also produced models based on a Bernoulli noise model by randomly distributing the two facies (clay and sand) on the simulation grid, with a proportion of sand ranging from 10% to 80%. Thirty realizations of each facies distribution produced a total of 240 (8×30) noise models. These models do not have any channelized structures; therefore, they can be used as a reference to quantify the influence of the organized structures like channels on the estimated Kx_{eff}, Ky_{eff}, and Kz_{eff} values. Figure 2a and 2b shows that the range of parameters investigated result in models with a variety of channelized structures and different connected patterns. We now set out to determine how these modifying properties affect the bulk effective vertical conductivities.

Determining the Bulk Effective Hydraulic Conductivity

The effective bulk hydraulic conductivity is estimated using flow-based upscaling. We perform flow-based upscaling to determine the bulk effective hydraulic

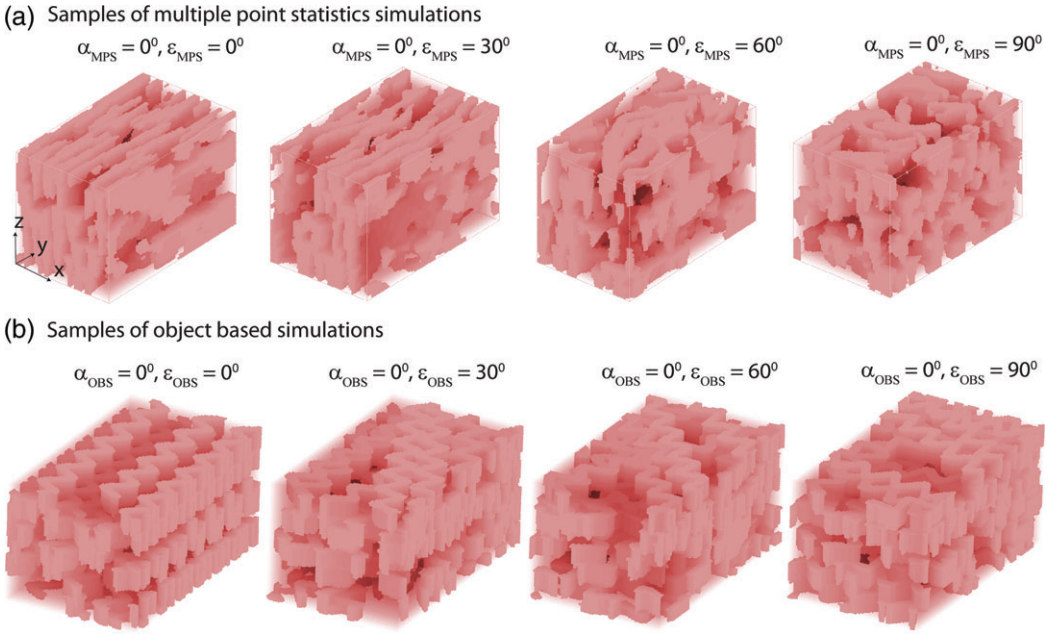

Figure 2. Samples of 3D geological units obtained from multiple-point statistics (MPS) simulation and object-based simulation (OBS). (a) Single realization obtained from MPS simulations by applying median rotation (α_{MPS}) = 0° and rotation tolerance (ε_{MPS}) = 0° to 90° to the 3D training image with 30% sand. (b) Single realization of OBS using sinusoidal objects and orientations of 0° with uniform distribution of minimum and maximum values identical to $\pm\varepsilon_{OBS}$. The proportion of sand in (a) and (b) is 30%.

conductivities in all three directions (Kx_{eff}, Ky_{eff}, and Kz_{eff}) for each geological setting. Note that the channels in all produced models are principally oriented in the y direction (Figure 1d). A steady-state groundwater flow model is used with each 3D facies model, with fixed head boundaries in the direction of interest and no flow boundaries in other directions. For example, in the calculation of Kz_{eff}, fixed head boundaries are defined on the upper and lower sides of the model and no-flow boundary conditions in the x and y directions (Renard and De Marsily 1997). The flux across the model, Q, is calculated using grid-cell centered finite difference algorithm with a conjugate gradient solver (MODFLOW 2005, Harbaugh 2005). The obtained flux value is then used to estimate K_{zeff} using Darcy's law: $Kz_{eff} = \frac{Q}{A \nabla H}$, where A is the surface area and H is the head. Three contrasts of hydraulic conductivity are used in the simulations: low (1 m/day for clay and 10^2 m/day for sand, contrast = 10^2), medium (1 m/day for clay and 10^3 m/day for sand, contrast = 10^3), and high (10^{-2} m/day for clay and 10^3 m/day for sand, contrast = 10^5). These are typical mean values of hydraulic conductivity used in other studies (e.g., Hunt and Idriss 2009; Huang et al. 2012). Numerical convergence of the flow models was validated, the mass balance errors being negligible for all simulations. The effect of different spatial arrangements of channelized structures on Kx_{eff}, Ky_{eff}, and Kz_{eff} is then evaluated by applying this groundwater simulation setting to 3D facies models with the three hydraulic conductivity contrasts, producing a total of 17,280 (5760×3) Kx_{eff}, Ky_{eff}, and Kz_{eff} values.

Results and Discussion

Bulk Effective Hydraulic Conductivity for MPS Models

Figure 3 shows the results of the flow-based upscaling for the MPS models. The variations in Kx_{eff}, Ky_{eff}, and Kz_{eff} values obtained as a function of the rotation tolerance, aspect ratios, and proportion of sand facies are presented in a similar way as Knudby et al. (2006) and Hunt and Idriss (2009). The upper and lower envelopes bulk effective values are the theoretical Wiener bounds (Wienner 1912) consisting of the arithmetic and harmonic mean hydraulic conductivity (KA and KH), respectively. Each point in the plots represents the average bulk effective hydraulic conductivity of 30 realizations, and for each color the different lines represent different ε_{MPS} values (rotation tolerance). The three columns correspond to results using MPS models with low, medium, and high hydraulic conductivity contrasts.

The plots in the first column (Figure 3a, 3d, and 3g) show that as the proportion of sand increases from 0% to 100%, Kx_{eff} and Ky_{eff} show more variability with changes in rotation tolerance and aspect ratio than Kz_{eff} estimates. A first observation is that there is almost no difference in the Kz_{eff} values obtained from 3D facies models with different ε_{MPS} values for a fixed channel aspect ratio. This behavior is consistent throughout all models obtained with MPS, and across different channel aspect ratios. The plots in the first and second rows (Figure 3a to 3f) show that by increasing the aspect ratio, there is an overall slight increase in Kx_{eff} and Ky_{eff} values. However, the values of Kz_{eff} are found to decrease with increasing aspect ratio (Figure 3g to 3i).

Table 1
List of Parameters Used in Simulation

Multiple-Point Simulation (MPS)			
Parameters	**MPS Model 1**	**MPS Model 2**	**MPS Model 3**
Size of the sketches in x and z directions (cells/pixels)	60×60	60×30	60×30
Dimension of the objects in the 2D sketches: width, depth (cells/pixels)	5, 10	10, 5	25, 5
Size of grids in 2D sketches	10×1 in x and z directions		
Channel aspect ratio (width/depth)	5	20	50
Number of grids in the 3D volumes from 2D sketches (e.g., Figure 2d) in x, y, and z directions	$60 \times 50 \times 60$	$60 \times 50 \times 30$	$60 \times 50 \times 30$
Rotation parameters applied to MPS models	$\alpha = 0^\circ$, $\varepsilon = 0^\circ$, 30°, 60°, 90°		
Number of grids in the simulations	$60 \times 100 \times 60$ in x, y, and z directions		
Size of grids in the simulation	$10 \times 10 \times 1$ in x, y, and z directions		

Object-Based Simulation (OBS)			
Parameters	**OBS Model 1**	**OBS Model 2**	**OBS Model 3**
Dimension of the sinusoidal object: length, width, depth, amplitude, wavelength (cells/pixels)	200, 5, 10, 4, 15	200, 10, 5, 4, 15	200, 25, 10, 4, 15
Orientations used in OBS models	[1]Uniform distribution of maximum and minimum values of $\pm 0^\circ$, $\pm 30^\circ$, $\pm 60^\circ$		
Number of grid cells in the geological simulations	$60 \times 100 \times 60$ in x, y, and z directions		
Dimensions of a grid cell in (m) in the simulation	$10 \times 10 \times 1$ in x, y, and z directions		

[1]In OBS models, rotation of channels is parameterized in a different manner than MPS models.

The proximity of profiles of Kx_{eff} and Ky_{eff} to KA bound indicates that the flow tends to move along the channelized layers in x and y directions. The profiles of Kx_{eff} are close to KA bound (Figure 3a to 3c). They show slight variation with rotation tolerance and channel aspect ratio, but there is no definite trend observed. Note that the channels are oriented in the y direction, so Ky_{eff} is expected to be close to KA bound irrespective of channel aspect ratio and rotation tolerance. The results shown in Figure 3d to 3f with Ky_{eff} overlapping in all cases confirm the expected behavior. As the contrast increases from low to high, the profiles tend to move away from KA bound. The profiles of Kz_{eff} values are closer to KH bound (Figure 3g to 3i), but the effect of channel aspect ratio is quite clear in this case. When the channels are deep (aspect ratio 5), it is more likely that the flow in the vertical direction will be along the connected channels like a parallel flow. However, in case of shallow channels (aspect ratio 50), the flow is expected to be perpendicular to the channels leading to Kz_{eff} values closer to KH bound.

The comparison of bulk effective hydraulic conductivities for MPS models with Bernoulli noise models shows that the channelized structures cause large variations in Kx_{eff} and Ky_{eff} (plots in first and second rows). However, for the vertical direction, the results from MPS and Bernoulli noise model overlap for lower proportions of sand until 30%. The overlap of results from MPS and Bernoulli noise model depends on the channel aspect ratio. For example, results from MPS with a channel aspect ratio of 5 significantly differ from the Bernoulli noise, except for the smallest sand proportions.

The profile of Kz_{eff} for MPS models with aspect ratio 50 seems fairly insensitive to the hydraulic conductivity contrast, yielding systematically lower values than the Bernoulli noise model, which indicates that when the channels are shallow and broad, the horizontal connectedness of the clay increases. Clay bodies then act as obstacles in the vertical movement of the flow. The Kz_{eff} values from MPS models with aspect ratios of 20 seem to regularly follow the profiles of the Bernoulli noise models. In this case, the influence of channels on the vertical flow is indistinguishable from that of the Bernoulli noise model, however they still significantly influence the horizontal flow.

The influence of ε_{MPS} on Kx_{eff}, Ky_{eff}, and Kz_{eff} is explicitly shown in the Figure S2. The arrangement of the figures is similar to Figures 3 and 4. It is clear from Figure S2(a) to S2(c) that there is an overall trend of Kx_{eff} increasing with the ε_{MPS} when the aspect ratio is 5 and 20. When the aspect ratio is 50, Kx_{eff} either remains similar or in some cases slightly decreases with increase in ε_{MPS}. Figure S2(d) to S2(f) shows that Ky_{eff}

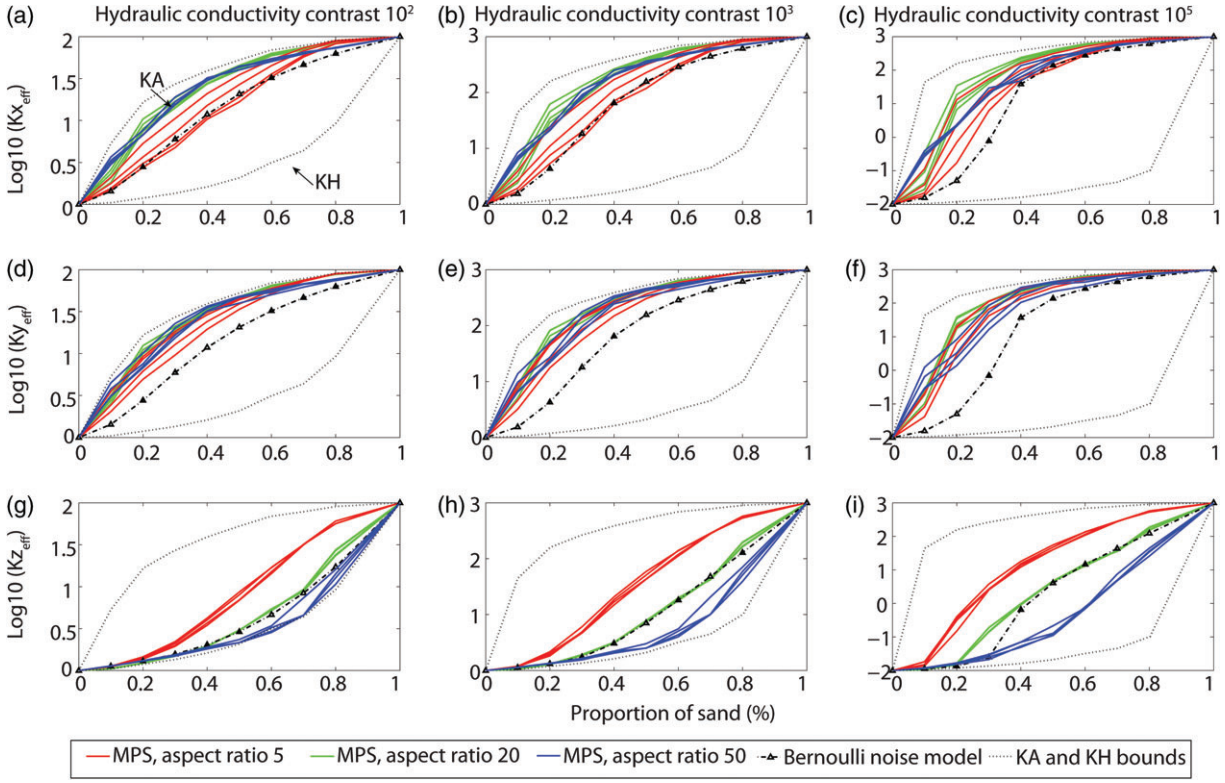

Figure 3. Estimated bulk effective hydraulic conductivities with different proportions of sand for different hydraulic contrasts for multiple-point statistics (MPS) simulations. Each line in the plots represents the mean value obtained from 30 realizations. For each color, the different lines represent different ε_{MPS} values. Bernoulli noise refers to models using random values without spatial structure. The Wiener bounds are shown in black.

presents a decreasing tend with an increase in ε_{MPS}. These observations indicate that by applying a rotation tolerance, the straight channels break and create obstacles for flow in the y direction (along channels), but it enhances flow in the x direction (across the main channel direction). As observed earlier in Figure 3, Kz_{eff} remains unaffected by ε_{MPS} except in some cases when there is a slight increasing trend, especially in case of channels with an aspect ratio of 50.

Bulk Effective Hydraulic Conductivity for OBS Models

The results of flow-based upscaling for the OBS simulations are presented in Figure 4, which has a similar layout than Figure 3. It is worth noting that the OBS models have long continuous channels, which contrasts to the often discontinuous channels of MPS as depicted in Figure 2a and 2b.

Figure 4a to 4c shows an increasing trend in Kx_{eff} with channel aspect ratio. When the hydraulic conductivity contrast is medium and high, there are large variations in Kx_{eff} between the curves that represent different ε_{OBS} values and different channel aspect ratios. On the contrary, Ky_{eff} obtained from OBS models with different aspect ratios and different ε_{OBS} values overlap (Figure 4d to 4f), which is explained by Ky_{eff} being computed along the channels direction, while Kx_{eff} is perpendicular to the channels. The way ε_{OBS} is applied in this study, the channels remain connected in the y direction (Figure 2b), so there is no significant change in Ky_{eff} values. When there is no variation in the orientation of the channel sets in different layers, surrounding lower permeability materials act as obstacles to the movement of flow in the x direction. As ε_{OBS} increases, the channels have an increasing likelihood of being oriented in directions other than y. When ε_{OBS} is 90°, the channels are as likely to be oriented in the x direction as the y direction, making it equally likely for connected flow pathways to develop in both directions (Figure 2b).

Figure 4g and 4h shows that the profiles of Kz_{eff} do not vary much with different ε_{OBS} values. It appears that the rotation of meandering channels do not affect the vertical flow paths significantly. When the hydraulic conductivity contrast is low to medium, Kz_{eff} decreases again with increasing aspect ratio. When the hydraulic conductivity contrast is high, the profiles of Kz_{eff} show large variations for different ε_{OBS} values. In case of low and medium channel aspect ratio, there is no definite trend between Kz_{eff} and ε_{OBS} values. For high aspect ratio, the channel geometry becomes similar to layered structures and the vertical flow becomes perpendicular to the channels, resulting into low Kz_{eff} values closer to KH bound (Figure 4i).

In the case of low hydraulic conductivity contrast, the profiles of Kz_{eff} obtained from Bernoulli noise model and OBS models overlap for aspect ratio 20, which is similar to the MPS results (Figures 3g and 4g). For

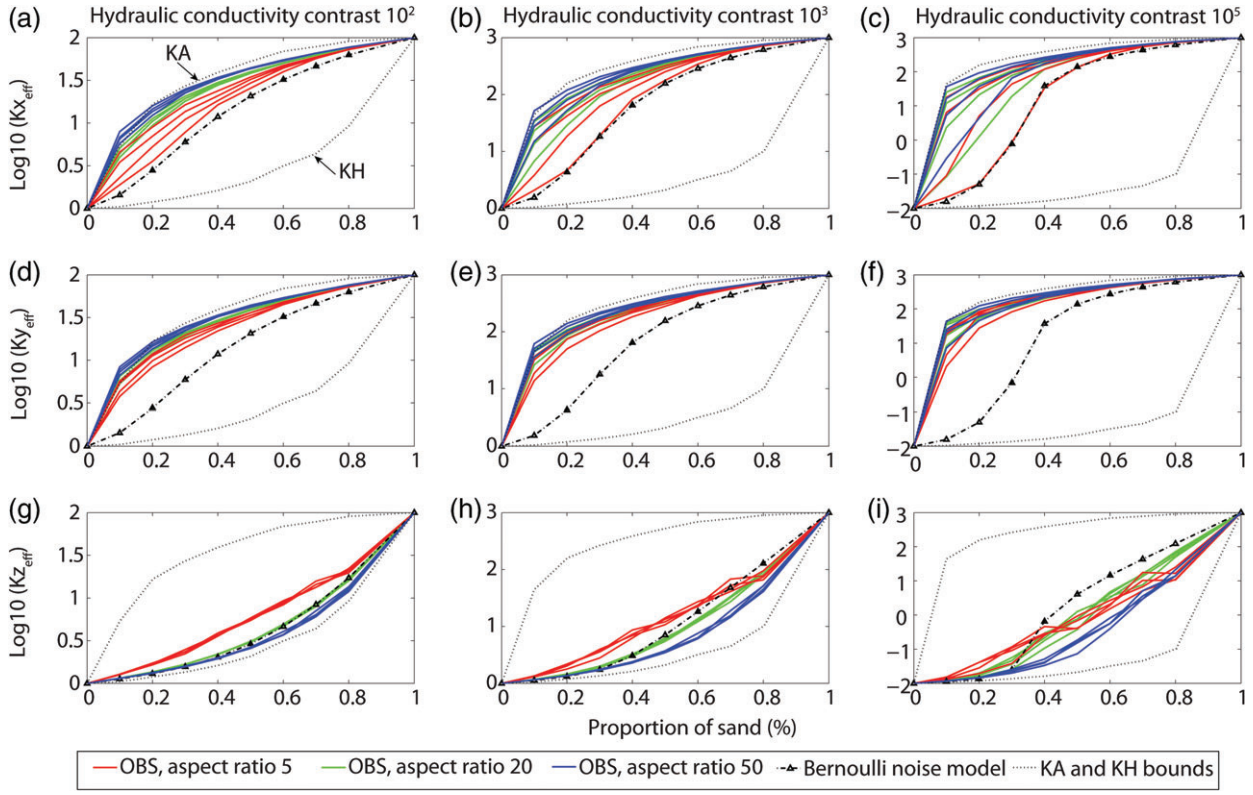

Figure 4. Estimated bulk effective hydraulic conductivities with different proportions of sand for different hydraulic contrasts for object-based simulations (OBS). Each line in the plots represents the mean value obtained from 30 realizations. For each color, the different lines represent different ε_{OBS} values. Bernoulli noise refers to models using random values without spatial structure. The Wiener bounds are shown in black.

medium hydraulic conductivity contrasts (Figure 4h), the OBS model with aspect ratios 20 and 50 overlap with Bernoulli model results until the sand proportion reaches about 30%. For higher sand proportions (30% to 80%), there is a significant difference between the Kz_{eff} values obtained from Bernoulli noise model and OBS model with channel aspect ratio 20. In case of high contrast (Figure 4i), there is a larger influence of channels orientations on the estimated Kz_{eff} values. The Kz_{eff} of the Bernoulli noise model is higher than any other model beyond a sand proportion of 40%. This indicates that low permeability material acts like a stronger barrier in case of structured channels than in case of channels being randomly located.

Figure 4 shows that the profiles of Kx_{eff} and Ky_{eff} are close to KA bound while Kz_{eff} is close to KH bound. Similar explanations as in the case of MPS results can also be applicable in this case. The flow moves along channels layers like a parallel flow in x and y directions, and perpendicular to channels in z direction. From Figure 4a and 4d, it can be seen that when the contrast is low, and Kx_{eff} and Ky_{eff} increase with the aspect ratio. This feature was not visible in the case of the MPS models shown in Figure 3. Note that in the OBS models, channels are more organized and continuous than the MPS models which is yielding to a definite dependency between Kx_{eff} *and* Ky_{eff} and aspect ratio.

The variation of Kx_{eff}, Ky_{eff}, and Kz_{eff} with ε_{OBS} are explicitly shown in Figure S3. Similar to what we observed in case of MPS models (Figure S2), Kx_{eff} increases with ε_{OBS} (Figure S3(a) to S3(c)), Ky_{eff} slightly decreases with ε_{OBS}, and Kz_{eff} either remains does not show a clear tendency when varying ε_{OBS}.

Sensitivity of Model Parameters

In the previous section, we observed that Kx_{eff}, Ky_{eff}, and Kz_{eff} are sensitive to various degrees to the proportion of sand, the channel aspect ratio, the rotation parameters, and the hydraulic conductivity contrast. In this section, we quantify this sensitivity to the different model parameters in MPS and OBS models with the help of tornado charts. The tornado charts are used to identify and rank the parameters according to their impact on the bulk effective hydraulic conductivities within a range of values.

As presented in Table 1, the range of parameters in MPS and OBS models is proportion of sand (10% to 80%), hydraulic conductivity contrasts (10^2, 10^3, and 10^5), channel aspect ratio (5, 20, and 50), and rotation tolerance (0°, 30°, 60°, and 90°). In the sensitivity analysis, we change one parameter at a time while keeping others at a fixed value. The fixed value of the parameters is selected as 40% for proportion of sand channels, 10^3 for hydraulic conductivity contrast, 20 for channel aspect ratio, and 60° for the rotation tolerance. For example, in order to perform sensitivity of the proportion of sand, its

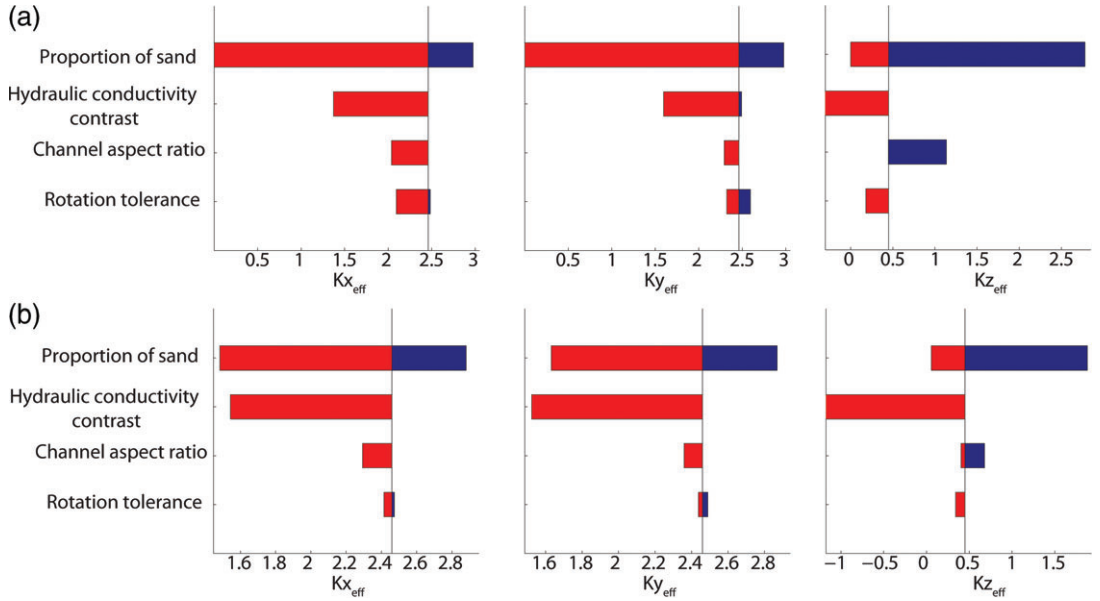

Figure 5. Tornado charts showing the 25th and 75th quantile of bulk effective hydraulic conductivity when varying the proportion of sand, hydraulic conductivity contrast, channel aspect ratio, and rotation tolerance on the bulk effective hydraulic conductivity obtained from (a) MPS models and (b) OBS models. The three columns correspond to the *x*, *y*, and z directions. One at a time, each parameter is assigned a range of values (10% to 80% proportion of sand; contrast = 10^2, 10^3, and 10^5; aspect ratio = 5, 20, and 50; rotation tolerance = 0°, 30°, 60°, and 90°), while the values of all other parameters are fixed. The fixed values of the parameters are proportion of sand = 40%, contrast = 10^3, aspect ratio = 20, and rotation tolerance = 60°.

value was varied from 10% to 80% while other parameters were kept constant (contrast = 10^3, aspect ratio = 20, rotation tolerance = 60°). Thus there are eight models (10% to 80% sand with other parameters fixed) and corresponding values of Kx_{eff}, Ky_{eff}, and Kz_{eff} obtained from 30 realizations. Those 240 (8×30) values of Kx_{eff}, Ky_{eff}, and Kz_{eff} are used in the tornado chart. Figure 5 presents the tornado charts ranking each model parameter according to how sensitive are Kx_{eff}, Ky_{eff}, and Kz_{eff} obtained from MPS and OBS models. In the tornado charts, the model parameters are listed in the decreasing order of their influence, such that the parameter with maximum sensitivity is displayed at the top. The bars represent the range between the 25th and 75th quantile of Kx_{eff}, Ky_{eff}, and Kz_{eff} values obtained by varying the corresponding parameter. We have not shown the maximum and minimum values as they may be affected by outliers. The results clearly show that the proportion of sand has the maximum influence on the bulk effective hydraulic conductivity values in all directions in both MPS and OBS models (Figure 5a and 5b, respectively), which is in agreement with the general concepts of percolation theory stating that the flow in a geological unit is primarily governed by the amount of high permeability materials. The hydraulic conductivity contrast is the second most important parameter to influence the bulk effective hydraulic conductivity values. Based on the high or low values of hydraulic conductivity contrast, the flow path may be either tortuous in attempting to pass only through high permeability material (high contrast case) or leak through the low permeability material (in the low contrast case). The influence of channel aspect ratio and rotation tolerance is overall minor for all cases considered, and particularly so for Kz_{eff}. In the MPS models (Figure 5a), the rotation tolerance has a slightly larger influence for Kx_{eff} and Ky_{eff} than for Kz_{eff}. However, in OBS models (Figure 5b), the channel rotation has very small impact in all three directions. These observations can be attributed to the fact that in OBS models, channels are continuous in the y direction and stacked on top of each other in the z direction, so the arrangement of lower permeability material acting as a flow barrier remains almost the same. While in MPS models the channels are less continuous and not so uniformly arranged; thus, channel rotation will likely change the arrangement of flow barriers (less permeability materials) more than in the case of OBS models. Overall, Figure 5 confirms that the rotation tolerance shows minimum influence on the vertical bulk effective hydraulic conductivity in both MPS and OBS models.

Conclusions

In this article, we perform a systematic sensitivity analysis based on numerical models to assess the influence of channels' morphology properties on flow properties (Kx_{eff}, Ky_{eff}, and Kz_{eff}) in channelized alluvial formations. The connectivity in the channels is controlled by the proportion of sand, the channel aspect ratio, by applying a set of rotations on the channels, and by the hydraulic conductivity contrasts between the facies. The results are presented across a range of channelized structures generated using multiple-point geostatistics and object-based methods.

The influence of morphological characteristics such as the channel rotation is found to be minor. The bulk properties such as the proportion of channels and the hydraulic conductivity contrast between channel and matrix play a dominant role. The role of channel aspect ratio (width/depth ratio) is significant. This said, the values of Kz_{eff} are found to be generally decreasing with increasing channel aspect ratio. We interpret that this occurs because the structures of high aspect ratio (broad and shallow channels) increases horizontal connectedness of the low permeability materials which acts like a barrier to the vertical flow.

We conclude that for problems where vertical flow is of interest (and not transport), it may not be critical to accurately replicate the detailed meander patterns of the channelized structures such as the channels sinuosity. Morphological channels properties that affect the vertical stacking of the structures, such as the channels width/depth ratio, can play a more significant role. However, the most important factors (proportion, contrast) are those that are not related to the detailed morphological properties of the channels. This study only applies to channel-like structures. Future investigation will focus on generalizing the study to any channel aspect ratio and also make it applicable in different settings such as deltaic or turbiditic systems. In this regard, the aspect ratio can be made more general by selecting the depth of the channels from a depth distribution function which can be normalized by a suitable value such as the thickness of the modeled domain. To generalize the study to different depositional environments, distributions on the high and low permeability materials have to be defined. The distributions functions will involve more parameters in addition to morphological parameters considered in this study. The influence of the combination of all parameters on the bulk effective hydraulic conductivities is an interesting avenue for future research on this topic.

Acknowledgments

This research was supported by the New South Wales State Government. The National Center for Groundwater Research and Training (NCGRT) is supported by the Australian Research Council and the National Water Commission. National ICT Australia (NICTA) is supported by the Australian Government through the Department of Communications and the Australian Research Council through the ICT Center of Excellence Program. We thank Dr Geoff Bohling and one anonymous reviewer for providing insightful comments that helped improving the manuscript significantly.

Supporting Information

Additional Supporting Information may be found in the online version of this article:

Figure S1. 2D view of object-based simulations (OBS). (a) to (c) represent three sets of cross section of OBS models with channels in an aquifer with aspect ratio 5, 20, and 50, respectively.

Figure S2. Estimated bulk effective hydraulic conductivities with ε_{MPS} values for different hydraulic contrasts for multiple-point statistics (MPS) simulations. Each line in the plots represents the mean value obtained from 30 realizations. For each color, the different lines represent different proportions of sand. (a) to (c) represent bulk effective hydraulic conductivities in x direction (Kx_{eff}), (d) to (f) represent bulk effective hydraulic conductivities in y direction (Ky_{eff}), (g) to (i) represent bulk effective hydraulic conductivities in z direction (Kz_{eff}).

Figure S3. Estimated bulk effective hydraulic conductivities with ε_{OBS} values for different hydraulic contrasts for object-based simulations (OBS). Each line in the plots represents the mean value obtained from 30 realizations. For each color, the different lines represent different proportions of sand. (a) to (c) represent bulk effective hydraulic conductivities in x direction (Kx_{eff}), (d) to (f) represent bulk effective hydraulic conductivities in y direction (Ky_{eff}), (g) to (i) represent bulk effective hydraulic conductivities in z direction (Kz_{eff}).

References

Andrade Jr, J.S., S.V. Buldyrev, N.V. Dokholyan, S. Havlin, P.R. King, Y. Lee, G. Paul, and H.E. Stanley. 2000. Flow between two sites on a percolation cluster. *Physical Review E* 62, no. 6: 8270.

Arpat, G.B., and J. Caers. 2007. Conditional simulation with patterns. *Mathematical Geology* 39, no. 2: 177–203.

Chen, X. 1997. Uncertainty analysis of the vertical aquitard hydraulic conductivity in a leaky aquifer system. *Environmental Geosciences* 4, no. 4: 186–191.

Dell'Arciprete, D., C. Vassena, F. Baratelli, M. Giudici, R. Bersezio, and F. Felletti. 2014. Connectivity and single/dual domain transport models: Tests on a point-bar/channel aquifer analogue. *Hydrogeology Journal* 22, no. 4: 761–778.

Deutsch, C., and T. Tran. 2002. FLUVSIM: A program for object-based stochastic modeling of fluvial depositional systems. *Computers & Geosciences* 28, no. 4: 525–535.

Falivene, O., L. Cabrera, J. Muñoz, P. Arbués Cazo, Ó. Fernández, and A. Sáez. 2007. Statistical grid-based facies reconstruction and modelling for sedimentary bodies. Alluvial-palustrine and turbiditic examples. *Geologica Acta* 5, no. 3: 199–230.

Fleckenstein, J.H., and G.E. Fogg. 2008. Efficient upscaling of hydraulic conductivity in heterogeneous alluvial aquifers. *Hydrogeology Journal* 16, no. 7: 1239–1250.

Gibling, M.R. 2006. Width and thickness of fluvial channel bodies and valley fills in the geological record: A literature compilation and classification. *Journal of Sedimentary Research* 76, no. 5: 731–770.

Guin, A., and R.W. Ritzi, Jr. 2008. Studying the effect of correlation and finite-domain size on spatial continuity of permeable sediments. *Geophysical Research Letters* 35: L10402. DOI:10.1029/2007GL032717.

Guin, A., R. Ramanathan, R.W. Ritzi, Jr., D.F. Dominic, I.A. Lunt, T.D. Scheibe, and V.L. Freedman. 2010. Simulating the heterogeneity in braided channel belt deposits: 2. Examples of results and comparison to natural deposits. *Water Resources Research* 46: W04516. DOI:10.1029/2009WR008112.

Haldorsen, H.H., and D.M. Chang. 1986. Notes on stochastic shales: from outcrop to simulation model. In *Reservoir*

Characterization, ed. L.W. Lake, and H.B. Carroll, Jr. Academic Press.

Harbaugh, A.W. 2005. MODFLOW-2005, the US Geological Survey Modular Ground-Water Model: The Ground-Water Flow Process. Reston, Virginia: US Department of the Interior, US Geological Survey.

Hart, D.J., K.R. Bradbury, and D.T. Feinstein. 2006. The vertical hydraulic conductivity of an aquitard at two spatial scales. *Ground Water* 44, no. 2: 201–211.

Harter, T. 2005. Finite-size scaling analysis of percolation in three-dimensional correlated binary Markov chain random fields. *Physical Review E* 72, no. 2: 026120.

Hill, E., and C. Griffiths. 2009. Describing and generating facies models for reservoir characterisation: 2D map view. *Marine and Petroleum Geology* 26, no. 8: 1554–1563.

Huang, L., R.W. Ritzi, and R. Ramanathan. 2012. Conservative models: Parametric entropy vs. temporal entropy in outcomes. *Groundwater* 50, no. 2: 199–206.

Hunt, A. 2001. Applications of percolation theory to porous media with distributed local conductances. *Advances in Water Resources* 24, no. 3: 279–307.

Hunt, A., and B. Idriss. 2009. Percolation-based effective conductivity calculations for bimodal distributions of local conductances. *Philosophical Magazine* 89, no. 22–24: 1989–2007.

Jha, S.K., A. Comunian, G. Mariethoz, and B.F. Kelly. 2014. Parameterization of training images for aquifer 3D facies modeling integrating geological interpretations and statistical inference. *Water Resources Research* 50: 7731–7749.

Knudby, C., J. Carrera, J.D. Bumgardner, and G.E. Fogg. 2006. Binary upscaling—the role of connectivity and a new formula. *Advances in Water Resources* 29, no. 4: 590–604.

Maharaja, A. 2008. TiGenerator: Object-based training image generator. *Computers & Geosciences* 34, no. 12: 1753–1761.

Mariethoz, G., and B.F.J. Kelly. 2011. Modeling complex geological structures with elementary training images and transform-invariant distances. *Water Resources Research* 47: W07527. DOI:10.1029/2011WR010412.

Moran, C., and S. Vink. 2010. *Assessment of Impacts of the Proposed Coal Seam Gas Operations on Surface and Groundwater Systems in the Murray-Darling Basin*, 4–5. Brisbane, Australia: Sustainable Minerals Institute.

Ramanathan, R., A. Guin, R.W. Ritzi, Jr., D.F. Dominic, V.L. Freedman, T.D. Scheibe, and I.A. Lunt. 2010. Simulating the heterogeneity in braided channel belt deposits: 1. A geometric-based methodology and code. *Water Resources Research* 46: W04515. DOI:10.1029/2009WR008111.

Renard, P., and G. De Marsily. 1997. Calculating equivalent permeability: A review. *Advances in Water Resources* 20, no. 5–6: 253–278.

Renard, P., J. Straubhaar, J. Caers, and G. Mariethoz. 2011. Conditioning facies simulations with connectivity data. *Mathematical Geoscience* 43, no. 8: 879–903.

Ronayne, M.J., and S.M. Gorelick. 2006. Effective permeability of porous media containing branching channel networks. *Physical Review E* 73, no. 2: 026305.

Ronayne, M.J., S.M. Gorelick, and J. Caers. 2008. Identifying discrete geologic structures that produce anomalous hydraulic response: An inverse modeling approach. *Water Resources Research* 44: W08426. DOI: 10.1029/2007WR006635.

Sanchez-Vila, X., A. Guadagnini, and J. Carrera. 2006. Representative hydraulic conductivities in saturated groundwater flow. *Reviews of Geophysics* 44, no. 3: RG3002.

Stauffer, D., and A. Aharony. 1992. *Introduction to Percolation Theory*. 2nd ed. London: Taylor and Francis.

Strebelle, S. 2002. Conditional simulation of complex geological structures using multiple-point statistics. *Mathematical Geology* 34, no. 1: 1–21.

Szymkiewicz, A. 2013. *Upscaling from Darcy Scale to Field Scale*. *Modelling Water Flow in Unsaturated Porous Media.* Berlin Heidelberg: Springer.

Wen, X.-H., and J.J. Gómez-Hernández. 1996. Upscaling hydraulic conductivities in heterogeneous media: An overview. *Journal of Hydrology* 183, no. 1: ix–xxxii. DOI: 10.1016/S0022-1694(96)80030-8.

Wienner, O. 1912. Abhandlungen der Mathematisch-Physischen Klasse der Koniglichen Sachsischen Gesellschaft der Wissenschaften. *Akademie des Wissenschaften Leipzig* 32: 509.